Available online at www.sciencedirect.com
SCIENCE DIRECT®
Journal of the European Ceramic Society 25 (2005) 3383–3392
www.elsevier.com/locate/jeurceramsoc

Effect of the composition and sintering process on mechanical properties and residual stresses in zirconia–alumina composites

Giuseppe Magnani[a,*], Aldo Brillante[b]

[a] *ENEA, Bologna Research Center, Via dei Colli, 40136 Bologna, Italy*
[b] *University of Bologna, Department of Physical and Inorganic Chemistry, 40136 Bologna, Italy*

Received 10 May 2004; received in revised form 10 September 2004; accepted 18 September 2004
Available online 7 December 2004

Abstract

Samples of zirconia-toughened alumina (ZTA) with small amounts of chromia and magnetoplumbite-type crystalline phase ($CeMgAl_{11}O_{19}$) have been prepared and processed under different conditions. Mechanical properties like hardness and fracture toughness were examined as a function of different parameters. As an example, fracture toughness was increased by the chromia addition, whereas platelets reinforcement addition suppressed the tetragonal zirconia (t-zirconia)–monoclinic zirconia (m-zirconia) transformation. In addition, transformability of the tetragonal zirconia and the residual stress in the alumina phase were examined by Raman and fluorescence piezo-spectroscopy, respectively. In particular, the extent to which t-zirconia transforms to m-zirconia was determined by Raman spectroscopy after Vickers indentation and the transformability was correlated to the fracture toughness. It was demonstrated that the monoclinic content and the toughness were correlated linearly and experimental results were compared with models already available for zirconia-based materials. On the other hand, residual stresses originated by transformation toughening mechanism were correlated to the transformability of the tetragonal phase.

Keywords: Al_2O_3/ZrO_2; Composites; Mechanical properties; Residual stresses; Sintering; $CeMgAl_{11}O_{19}$

1. Introduction

Zirconia-toughened alumina (ZTA) has been the subject of extensive research[1,2] because it couples a high toughness, with the peculiar properties of alumina, i.e. very good resistance to wear and chemical stability. All these characteristics have qualified ZTA for cutting application and make alumina–zirconia composites a very promising candidate as material for implant applications, also because alumina and zirconia separately are already familiar to the biomaterials community. In addition, ZTA ceramics have been studied in the past two decades in order to establish which toughening mechanism was predominant in this material. Several studies demonstrated that stress-induced transformation toughening and microcraking toughening were responsible of fracture toughness improvement.[3–7]

Focusing the attention on the transformation toughening mechanism, it is well known that tetragonal zirconia transformability depends on characteristics like grain size, type and amount of stabilizer and sintering conditions. In fact, Garvie[8] reported that grain size of tetragonal zirconia has to be maintained over a critical size to reach a high value of fracture toughness, while different oxides (Nb_2O_5, Ta_2O_5, Sc_2O_3, Er_2O_3, Gd_2O_3) were tested in order to increase the metastability of the tetragonal phase by means of variation of the *c*/*a* ratio of the elementary cell.[9–13] Furthermore, platelets-reinforced zirconia materials have been recently developed with secondary phase constituted by compounds with magnetoplumbite-type structure with the aim to increase toughness through crack deflection mechanism.[14–18]

* Corresponding author.
E-mail address: giuseppe.magnani@bologna.enea.it (G. Magnani).

0955-2219/$ – see front matter © 2004 Elsevier Ltd. All rights reserved.
doi:10.1016/j.jeurceramsoc.2004.09.025

The analytical methods used to evaluate transformability are X-ray diffraction, Raman and fluorescence spectroscopy. The main difference between the two methods is that XRD analysis is performed on fracture surface whereas Raman analysis can be directly performed around cracks originated from Vickers indentations to obtain a map with a spatial resolution as low as 1 μm.[19,20] With the same spatial resolution it is also possible to evaluate the stress induced by the t–m transformation in ZTA-based materials by means of the fluorescence piezo-spectroscopy. Using this analytical technique, Gregori et al.[21] has already demonstrated that the final stress state of the alumina matrix is governed only by the extent of the transformation of the zirconia particles, while Merlani et al.[22] studied grains size and cooling rate effects on compressive stress in alumina–zirconia composites.

In this paper, mechanical properties (hardness, fracture toughness) of ZTA composites, obtained in different conditions in terms of composition and sintering process, were analyzed as a function of the sintering process, stabilizer content, zirconia–alumina weight ratio, chromia addition and a new magnetoplumbite-type crystalline phase ($CeMgAl_{11}O_{19}$) content. In addition, tetragonal phase transformation induced by Vickers indentation was correlated to the fracture toughness by means of Raman spectroscopy, while stress of the alumina matrix originated by t–m transformation was determined by fluorescence piezospectroscopy and correlated to the transformability of the tetragonal phase.

2. Experimental procedure

Powders of yttria-stabilized zirconia (3YB, Tosoh, Japan), monoclinic zirconia (TZ0, Tosoh, Japan), alumina (Baikalox SM8, Baikowski Chimie, France) and chromia (Carlo Erba, Italy) were wet-mixed in a Turbula mixer using water as solvent. To obtain platelets reinforcement, $CeMgAl_{11}O_{19}$ was also added to the mixture. It was first obtained by coprecipitation method starting from $Ce(NO_3)_3{\cdot}6H_2O$, $Mg(NO_3)_2{\cdot}6H_2O$, $Al(NO_3)_3{\cdot}6H_2O$ (Carlo Erba, Italy) and ammonia as coprecipitating agent. Calcination of hydroxides species were performed at 900 °C and crystalline phase was finally achieved at 1500 °C, as reported in Fig. 1. This compound was subsequently mixed with the remaining constituents of the system.

The green bodies were made by means of die pressing at 60 MPa followed by CIP at 100 MPa. Pressureless sintering was performed in flowing air in the range 1450–1550 °C depending on the composition. Post-sintering treatment constituted by hot isostatic pressing (HIP) was applied on some samples to investigate the effects of different sintering processes on the transformability of the tetragonal phase. In Table 1 composition and sintering parameters of each sample are summarized.

Densities of sintered samples were determined by Archimedes's method. X-ray diffraction method (Model PW 1710 and PW 1820, Philips, using Ni filtered Cu Kα radiation, at 40 KV and 30 mA) was used to evaluate crystallographic composition and to calculate lattice parameters of the tetragonal phase. Hardness (*HV*) and fracture toughness (K_{Ic}) were determined by means of Vickers indentation with a load ranging from 96 N to 198 N (10 indentations for each load). To calculate fracture toughness, the formula proposed by Niihara for Palmqvist crack was used:[23]

$$K_{Ic} = \frac{0.035(Ha^{1/2})(3E/H)^{0.4}(l/a)^{-0.5}}{3} \quad (1)$$

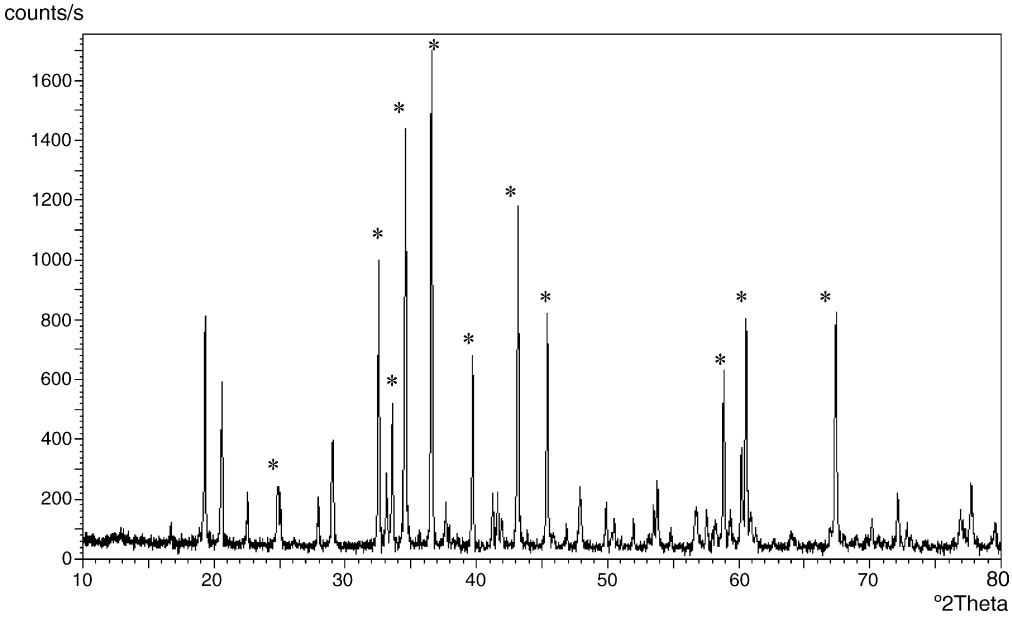

Fig. 1. XRD patterns of $CeMgAl_{11}O_{19}$ (JCPDS card 26-0872) obtained by coprecipitation/calcination method.

Table 1
Composition and sintering parameters of the samples examined

Sample ID	ZrO_2 (3YB) (wt.%)	ZrO_2 (TZ0) (wt.%)	Al_2O_3 (wt.%)	Cr_2O_3 (wt.%)	$CeMgAl_{11}O_{19}$ (wt.%)	Sintering	HIP (100 MPa)
AZ1	60		40			1450 °C × 1 h	
AZC4	33.6	16.4	49.5	0.5		1450 °C × 1 h	1450 °C × 2 h
AZC112	26.9	13.1	59.5	0.5		1500 °C × 1 h	
AZ16	33.6	16.4	50			1450 °C × 1 h	1450 °C × 2 h
AZ17	50		50			1450 °C × 1 h	1450 °C × 2 h
AZC18	26.9	13.1	59.5	0.5		1500 °C × 1 h	1450 °C × 2 h
AZC25	33.6	16.4	49.5	0.5		1450 °C × 1 h	
AZ26	26.9	13.1	60			1500 °C × 1 h	
AZ35	50		50			1450 °C × 1 h	
AZ38	33.6	16.4	50			1450 °C × 1 h	
AZC42	50		50	0.5		1450 °C × 1 h	
AZ60	41.8	8.2	50			1450 °C × 1 h	
AZCe20	26.9	13.1	40		20	1550 °C × 1 h	
AZCe20HP	26.9	13.1	40		20	1550 °C × 1 h	1450 °C × 2 h

This formula was used within the whole range of the applied load because we have previously demonstrated that the conditions of the Palmqvist crack model were always satisfied.[24]

Finally, Raman spectra were collected around Vickers indentation using the single grating spectrograph Renishaw System 1000 equipped with a suitable notch filter and a CCD detector. Raman scattering was excited with a Ar^+ laser at wavelength of 514.5 nm; the laser output power of 25 mW was reduced by means of neutral optical filters (form 50% to 90%) to avoid thermal damage of the sample. The point to point variation of the Raman spectra along the direction of the apex of the Vickers indent was obtained by moving the sample with steps of 20 μm using an *x*–*y* motorized stage. By using a 50× objective a spatial resolution of 1.2 μm was reached. Fluorescence piezo-spectroscopy measurements were performed with the same spectrometer, excitation and spatial resolution of Raman experiments, by mapping the peak positions of R_1 and R_2 ruby luminescence bands of Cr^{3+} centres of alumina.

3. Results and discussion

3.1. Effects of the sintering and composition on material properties

In Table 2 densities, hardness and fracture toughness of each sintered sample are reported. Above all, it should be noticed that the density is always close to the theoretical value (T.D.), independently of composition and sintering process. In the following paragraphs the effects of thermal cycle, stabilizer content, chromia on the mechanical properties will be discussed.

3.1.1. Hot isostatic pressing

Hot isostatic pressing caused always a reduction of fracture toughness, more evident at low level of stabilizer content (compare the results of the samples AZ16–AZ38, AZ35–AZ17 and AZC4–AZC25), while it was effective to increase hardness (see the same samples). The main reason of fracture toughness decreasing is that this additional heat treatment led to grain growth of the tetragonal phase (Fig. 2a and b) and hence partial t–m transformation of the zirconia grains that reduces the amount of tetragonal phase available for the transformation, as shown in Fig. 3a and b, where XRD spectra of AZ38 and AZ16 are reported.

3.1.2. Stabilizer content

The effect of the stabilizer (Y_2O_3) amount was investigated through preparation of samples having a zirconia/yttria molar ratio of 97/3, 3Y (AZ35), 97.5/2.5, 2.5Y (AZ60) and 98/2, 2Y (AZ38), respectively. As shown in Table 2, fracture toughness reached a maximum value of 8.1 MPa $m^{1/2}$ with the lowest content of stabilizer, while with yttria content of 3 mol% and 2.5 mol%, K_{Ic} did not exceed 6.0 MPa $m^{1/2}$. To

Table 2
Density and mechanical properties of the sintered samples (±standard deviation)

Sample ID	Density (T.D.%)	Hardness (GPa)	Fracture toughness (MPa $m^{1/2}$)
AZ1	99.8	15.0 ± 0.2	6.1 ± 0.1
AZC4	99.9	16.2 ± 0.2	6.7 ± 0.2
AZC112	99.9	15.9 ± 0.3	6.9 ± 0.2
AZ16	99.9	16.1 ± 0.2	6.2 ± 0.3
AZ17	99.6	15.9 ± 0.3	5.8 ± 0.1
AZC18	99.8	16.3 ± 0.2	6.5 ± 0.1
AZC25	99.4	15.5 ± 0.1	9.1 ± 0.8
AZ26	99.7	16.3 ± 0.3	7.0 ± 0.2
AZ35	99.3	14.9 ± 0.5	6.0 ± 0.1
AZ38	99.2	15.4 ± 0.2	8.1 ± 0.1
AZC42	99.4	15.2 ± 0.5	6.4 ± 0.2
AZ60	99.9	15.7 ± 0.3	5.6 ± 0.2
AZCe20	99.8	15.2 ± 0.2	7.0 ± 0.4
AZCe20HP	99.8	15.3 ± 0.3	6.1 ± 0.1

Table 3
Lattice parameters and *c*/*a* ratio of AZ35, AZ60, AZ38

Sample ID	*a* (nm)	*c* (nm)	Tetragonality (*c*/*a*)	Tetragonal phase (vol.%)	Cubic phase (vol.%)
AZ35 (3Y)	0.50964	0.51805	1.0165	98.7	1.3
AZ38 (2Y)	0.50958	0.51851	1.0175	100	
AZ60 (2.5Y)	0.50982	0.51850	1.0170	94.6	5.4

understand this behaviour, lattice parameters *c* and *a* (*c*/*a* ratio) must be taken into consideration. In fact, it is well-known that the loss of tetragonality (a lower *c*/*a* ratio) is related to an increased stability of the tetragonal phase which causes a decrease of fracture toughness. In particular, Yoshimura et al.[25] reported that *c*/*a* ratio is independent of the dopant size (though it was not confirmed by Tien[10] and Jang et al.[11]), but dependent on the content of stabilizer. This was also confirmed in our case, as reported in Table 3. However, besides the *c*/*a* ratio, crystallographic composition (Table 3) has also to be considered to explain the behaviour of fracture toughness as function of yttria content (Fig. 4). In fact, the difference between AZ38 and the other samples is due to the different *c*/*a* ratio, while the difference between AZ35 and AZ60 is due to the different amount of the tetragonal phase available for the transformation.

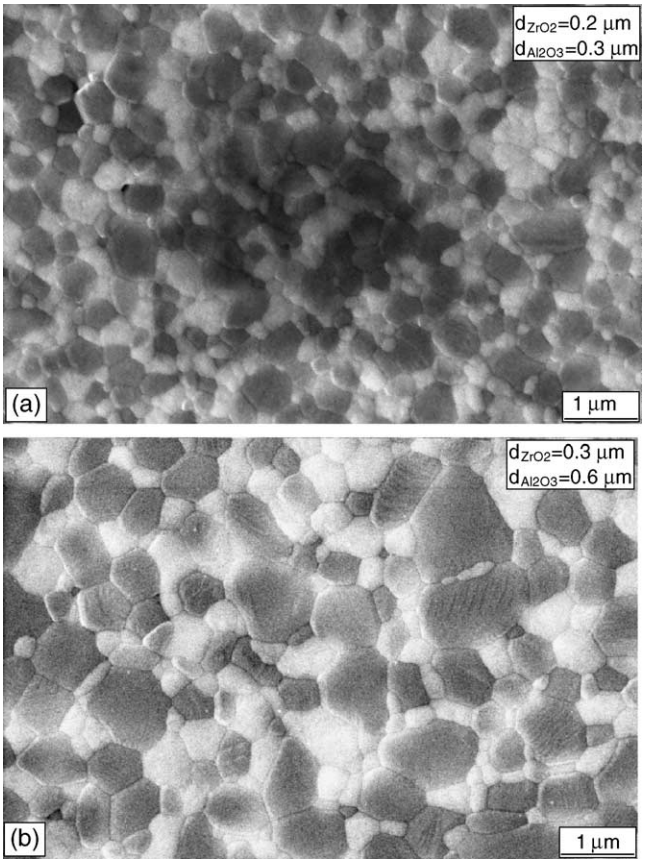

Fig. 2. SEM image of the microstructure of (a) AZ38 and (b) AZ16 (white grains: zirconia; black grains: alumina). Average grain size of zirconia and alumina are reported in the figure.

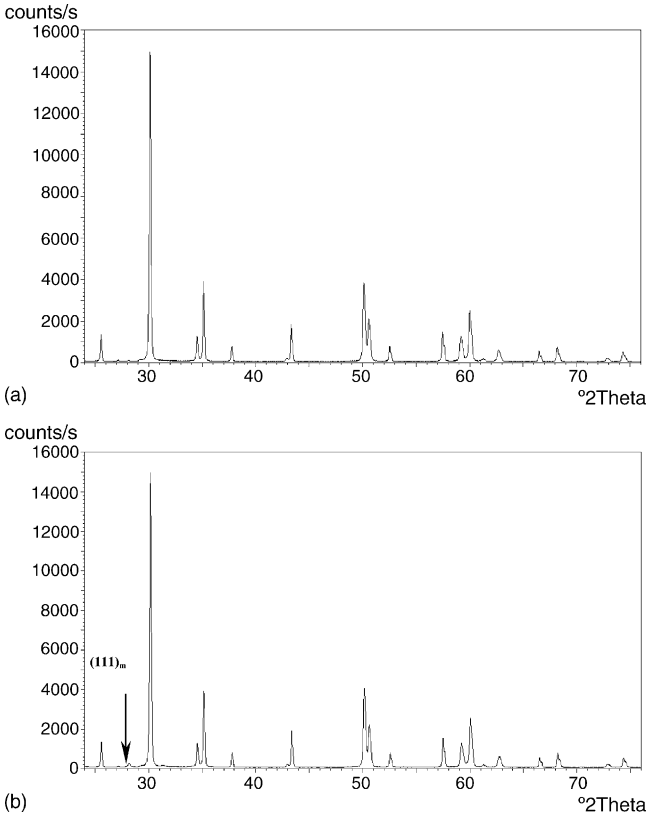

Fig. 3. XRD spectra of (a) AZ38 and (b) AZ16. Amount of monoclinic phase (2 vol.%) was determined following Polymorph method (prENV 14273-2001).

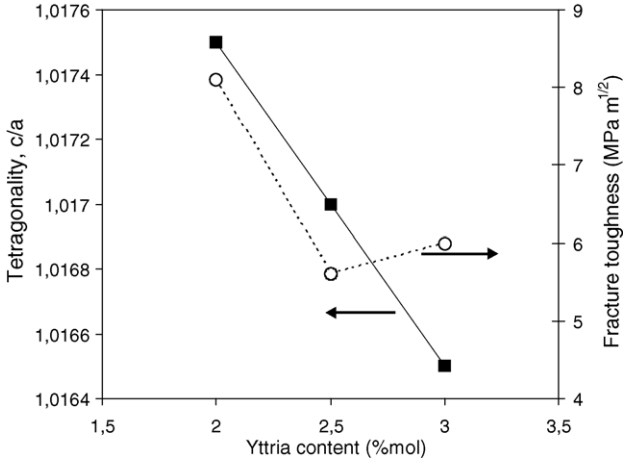

Fig. 4. Correlation between tetragonality–fracture toughness and stabilizer content.

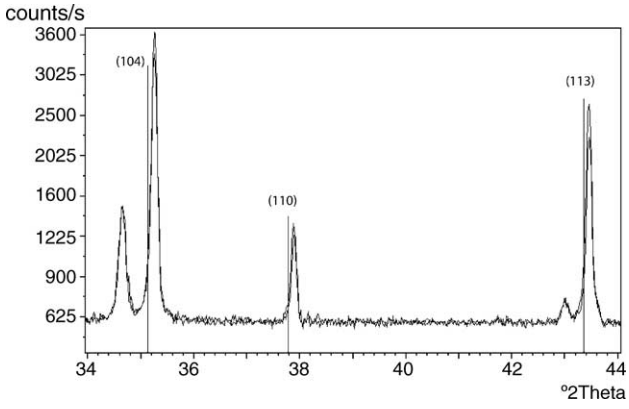

Fig. 5. XRD patterns of 0.5 wt.% chromia-doped ZTA ceramics. Straight lines are the peak positions of pure sintered alumina (JCPDS card 46-1212).

3.1.3. Chromia

Chromia's effects on mechanical properties of alumina and alumina–zirconia composites (ZTA) have already been studied. It is well known that Cr_2O_3 forms a isovalent solid solution with Al_2O_3 over the full range of compositions, with a great influence on microstructural evolution. On the other hand, Cr^{3+} is hardly soluble in ZrO_2 and the solubility depends on the preparation conditions.[26,27] Arahori and Whitney[28] found that hot pressed ZTA showed higher value of fracture toughness and hardness with a chromia/alumina weight ratio of 0.1. On the contrary, in chromia–zirconia (3Y-TZP) composites the maximum value of fracture toughness was achieved with a volume ratio of 0.3.[29] Finally, Riu et al.[30] demonstrated that hot pressed alumina-chromia composites had hardness dependent on chromia content. In our case the chromia content was fixed at 0.5 wt.% to limit weight loss due to CrO_3 vaporization[31] during pressureless sintering and therefore we were not able to put in evidence any variation of mechanical properties due to different chromia content. X-ray diffraction measurements were performed, but we were not able to detect any chromium containing phase; in agreement to literature, we found only a little effect on alumina cell parameters, because of the formation of a solid solution (Fig. 5).[28] As example (0 0 6) peak and (3 0 0) were, respectively, shifted of 0.0054° and 0.0214° (2Θ), a value corresponding to an increase of alumina cell parameters *c* and *a* of 0.01% and 0.03%, respectively. In conclusion, we could only evaluate whether chromia addition affected toughness and/or hardness. On the basis of the experimental data reported in Table 2, we can argue that chromia addition led to an enhancement of fracture toughness both in the pressureless sintered samples (AZC25 versus AZ38 and AZC42 versus AZ35) and in the hipped samples (AZC4 versus AZ16). It can also be noticed that this is not true when zirconia–alumina weight ratio increase from 50:50 to 40:60. In this case, fracture toughness was quite insensitive to the chromia doping (AZ26 versus AZC112). On the other hand, it can also be concluded that hardness was not greatly influenced by the chromia addition independently of the composition.

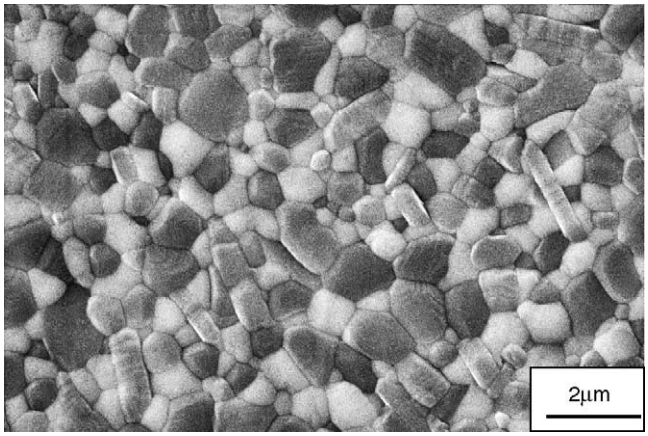

Fig. 6. Microstructure of 20 wt.% $CeMgAl_{11}O_{19}$-doped ZTA sintered sample (AZCe20). White grains: zirconia; black grains: alumina; platelets: $CeMgAl_{11}O_{19}$.

3.1.4. Cerium-based magnetoplumbite type phase

Magnetoplumibite type structure shows a hexagonal lattice with an anisotropic growth which is suitable to form in situ rodlike particles. These rodlike particles can act as toughening agents to improve the mechanical properties of the composites, normally without any sintering problems due to their in situ formation during densification. In our case, we preferred to add this phase directly to ZTA composites in order to reach a sintered density as close as possible to the theoretical value (Table 2). In Fig. 6 the microstructure of the sintered sample AZCe20 is reported where the grains with high aspect ratio are constituted by $CeMgAl_{11}O_{19}$. Aluminates such as $CeMgAl_{11}O_{19}$ have common properties like lower hardness and Young's modulus than those of corundum. These properties of a composite decrease with increasing content of aluminates, giving rise to reduced constraint on the ZrO_2 from the surroundings. Therefore, ZrO_2 toughening eventually becomes less effective. Obviously, there is a compromise of aluminates content for gaining optimal mechanical properties. In our case, we characterized only ZTA composites containing 20 wt.% of $CeMgAl_{11}O_{19}$. Future work will be aimed to investigate the effect of the cerium-based compound content on the fracture toughness. Overall fracture toughness of samples doped with this phase (AZCe20 and AZCe20HP) is comparable with that of ZTA samples obtained with the same sintering process, AZ38 and AZ17, respectively. It is confirmed that tetragonal transformation toughening is less effective in AZCe20 samples irrespective of the sintering process, while it is partially compensated by platelets toughening through crack deflection mechanism, as clearly reported in Fig. 7.

3.1.5. Zirconia–alumina weight ratio

Samples with different zirconia–alumina weight ratio were also prepared, as reported in Table 1. The effects of different zirconia–alumina ratios on mechanical properties are in agreement with previous studies on these materials. In fact, increasing zirconia content produced an increment

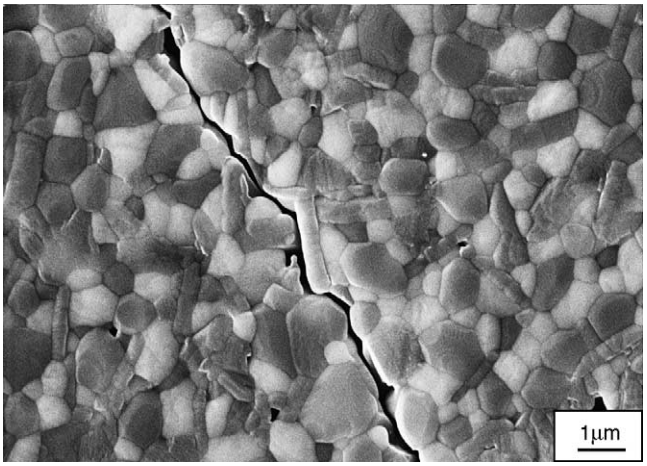

Fig. 7. Crack propagation in platelets reinforced ZTA material (AZCe20).

of the fracture toughness (AZ1 and AZ35 in Table 2), while a more evident decrease was achieved when alumina content raised up to 60 wt.%. Furthermore, this sample (AZ26) showed a higher hardness than sample AZ38 with 50 wt.% as alumina content. In the chromia-doped ZTA sintered samples, fracture toughness raised when zirconia–alumina weight ratio content was increased and this increment was more evident in the pressureless sintered samples (compare values of AZC25–AZC112 with AZC4–AZC18).

Table 4
Transformability's parameters of the sintered samples

Sample ID	V_f	d (μm)	$V_f(d)^{1/2}$ $(\mu m)^{1/2}$
AZ16	0.31 ± 0.03	55.1 ± 7.8	2.26
AZ17	0.26 ± 0.06	44.8 ± 1.5	1.75
AZ35	0.32 ± 0.03	44.6 ± 2.7	2.14
AZ38	0.51 ± 0.06	82.6 ± 22.0	4.61
AZ60	0.24 ± 0.05	42.6 ± 11.1	1.57

3.2. Raman analysis

In zirconia-based materials, fracture toughness is related to the transformability of tetragonal phase according to the equation proposed by McMeeking and Evans:[32]

$$K_{Ic} = K_{Ic}^{m} + \left(\frac{\eta V_f \Delta V E \sqrt{d}}{1 - \nu} \right) \quad (2)$$

where K_{Ic}^{m} is the toughness of the material without tetragonal to monoclinic transformation, η is a constant, V_f is the volumetric fraction of the transformable tetragonal phase, ΔV is the lattice dilatation associated to the transformation (4.7%), E is the Young modulus, d is the transformation zone size (TSZ) and ν is the Poisson's ratio. Because η, ΔV, ν and E are constant, fracture toughness is function of $V_f(d)^{1/2}$. The latter parameter can be determined by means of Raman analysis following the method proposed by Katagiri et al.,[33] which is based on the elaboration of the data coming from a spatial mapping of the sample performed in the direction perpendicular to the crack, as reported in Fig. 8a. Example of Raman spectra obtained at different distances from the indentation apex, are shown in Fig. 8b. The monoclinic fraction has been estimated from the relative intensities of the monoclinic doublet (bands at 181 cm^{-1} and at 192 cm^{-1}) with respect to the tetragonal band at 145 cm^{-1}. From the calculated gaussian

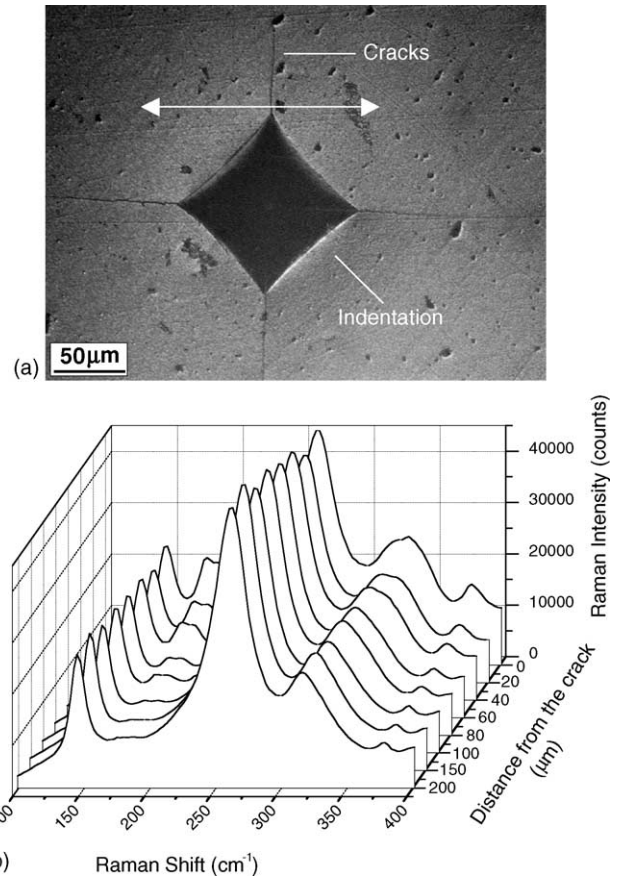

Fig. 8. (a) Low magnification image with indication of the mapping paths. (b) Raman spectra acquired at different distance from the crack.

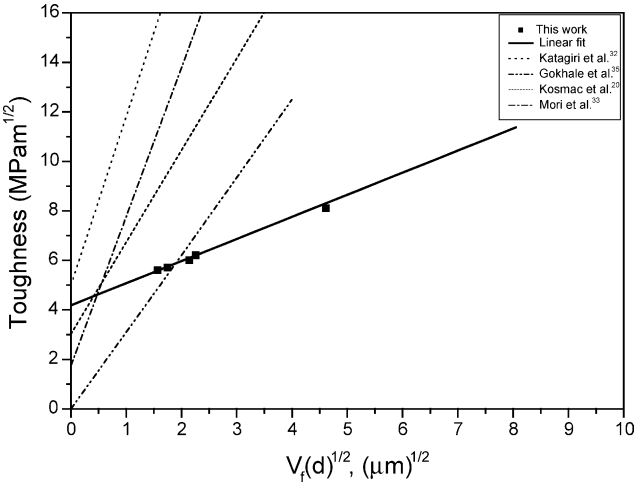

Fig. 9. Fracture toughness of sintered samples as a function of the transformability.

distribution of the monoclinic fraction, with reference to the edge of the Vickers indent, V_f and d have been obtained.[33] Furthermore, we took in account the samples having the same zirconia–alumina weight ratio in order to compare sintered samples homogeneous from the zirconia and alumina content point of view (Table 4).

The data reported in Table 4 were related to the values of fracture toughness shown in Table 2 and a linear fit, based on of Eq. (2), is reported in Fig. 9. With the determination of η and K_{Ic}^{m}, we were able to demonstrate that the fracture toughness is mainly influenced by the transformation of the tetragonal phase. In fact, from the linear slope, with $\Delta V = 0.047$,

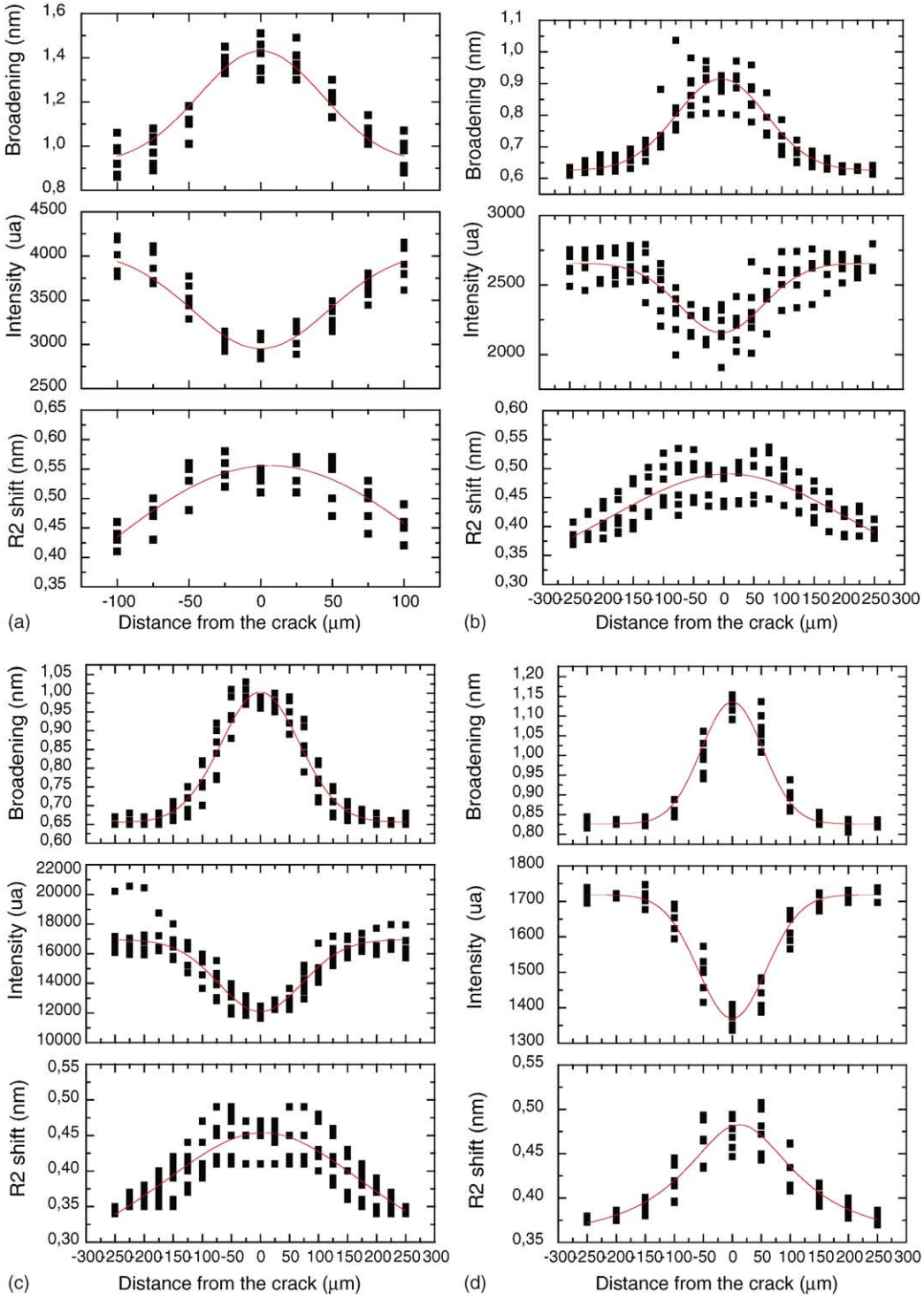

Fig. 10. R_2 band broadening, intensity and shift as a function of distance from the crack in (a) AZ16, (b) AZ17, (c) AZ26, (d) AZ38, (e) AZ60 and (f) AZCe20.

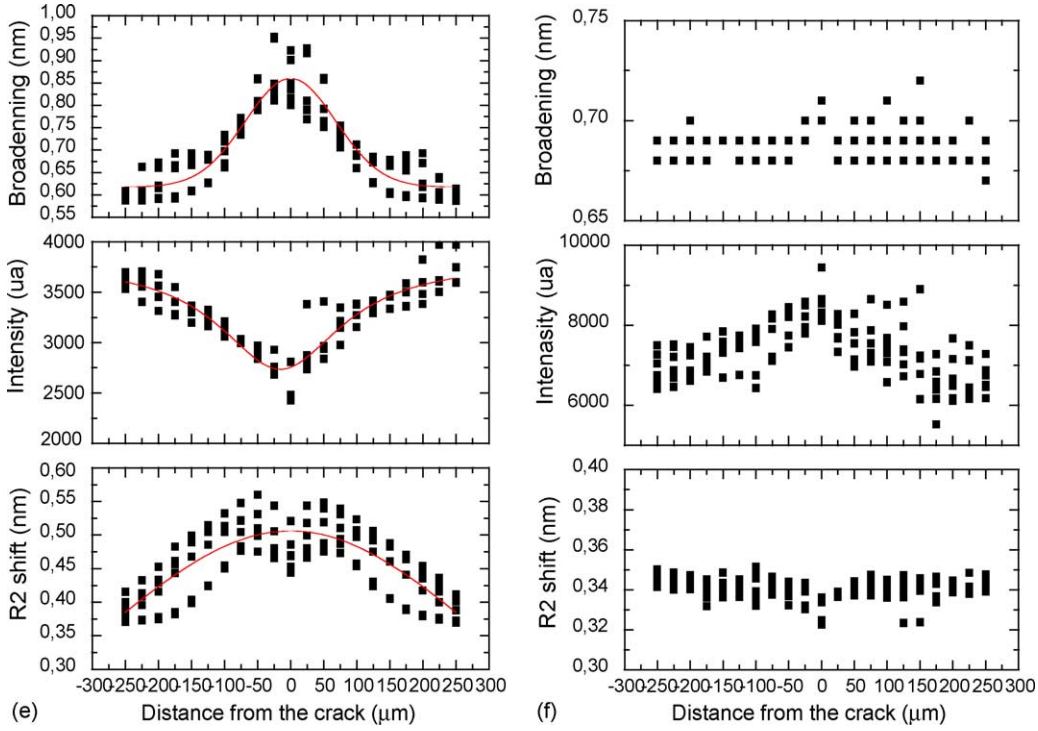

Fig. 10. (*Continued*).

$E = 305$ GPa (determined by resonance frequency method) and $\nu = 0.26$ (calculated by rule of mixture), we determined $\eta = 0.46$, which is included in the range 0.22–0.55 indicated by Mori et al.,[34] and $K_{Ic}^{m} = 4.2\ \text{MPa m}^{1/2}$, which is very close to the value ($4\ \text{MPa m}^{1/2}$) pointed out by Swain and Rose.[35] The difference between the slope of the linear fits previously reported by other authors[20,33,34,36] and shown for comparison with our experimental results in Fig. 9 is due to the fact that each fit is related to the data of different zirconia-based materials (different in the composition and/or in the manufacturing process) where fracture toughness is differently affected by the transformability.

3.3. Fluorescence piezo-spectroscopy

As already mentioned, alumina stress strains associated to the t–m transformation in a zirconia–alumina composite can be determined by means of fluorescence piezo-spectroscopy. In fact, the chromium ions, Cr^{3+}, are substitutional of the Al^{3+} ions and they give origin to sharp and characteristics fluorescence peaks also in polycrystalline materials. If a stress, applied or residual, acts on the system, the peaks at 693 nm (R_1) and 694.25 nm (R_2) are shifted.[37] A positive shift implies tension and a negative one implies compression acting on the alumina matrix. In our case, we performed a spatial mapping in the directions already showed in Fig. 8a, and we analyzed the resulting fluorescence spectra in order to obtain a correlation between characteristics of the R_2 band (wavelength shift, peak broadening and peak intensity) and distance from the indentation apex. The instrumental shift due to the variations in room temperature was also corrected by simultaneously monitoring a characteristic Neon line at 693.14 nm, close to the R lines. Experimental points were analyzed and interpolated by means of a Gaussian curves originated by a Lorentzian fit. These curves showed the maximum value in correspondence of the indentation apex as clearly reported in Fig. 10. All samples exhibited a positive shift due to the t–m transformation except AZCe20 where it was greatly suppressed, as already mentioned.

In ZTA-based materials residual stresses can be originated during cooling in the sintering process due to the different coefficient of thermal expansion (CTE) of the species, σ_{cte}. Furthermore, t–m transformation induced by surface machining or Vickers indentation can also lead to an internal stress that depends on the transformability, σ_{trans}. The available equations to calculate stresses are based on the correlation between the change in frequency, $\Delta\nu$, and the piezo-spectroscopy coefficients for the a and c directions relating frequency to stress, Π_{ij}. Here the equation proposed by Ma and Clarke is reported:[38]

$$\langle \Delta\nu \rangle = \tfrac{1}{3}(2\Pi_{11} + \Pi_{33})\langle \sigma_{ii}^{i} \rangle_{A} \tag{3}$$

where $\langle \sigma_{ii}^{i} \rangle_{A}$ is the hydrostatic stress, while Π_{11} and Π_{33} were previously measured at room temperature to have values of 2.75 and $2.10\ \text{cm}^{-1}\ \text{GPa}^{-1}$, respectively.[39] This equation was used to calculate the hydrostatic stresses σ_{cte} and σ_{trans} on the basis of the R_2 band shift measured before and after Vicker indentation, respectively. These values together to the overall hydrostatic stress, σ_{tot}, are reported in Table 5. In this manner, we are able to put in evidence that t–m transformation

Table 5
Residual stress of the alumina matrix due to CTE mismatch and tetragonal–monoclinic transformation

Sample ID	σ_{cte} (MPa)	σ_{trans} (MPa)	σ_{tot} (MPa)
AZ16	−998	159	−839
AZ17	−1069	294	−775
AZ26	−795	302	−493
AZ38	−1275	267	−1008
AZ60	−916	331	−551

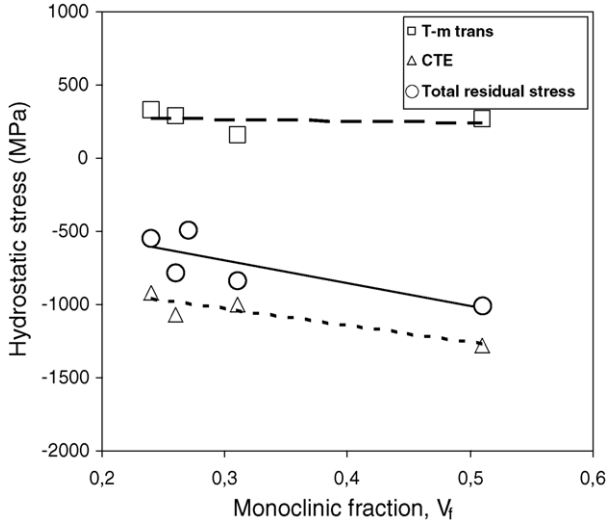

Fig. 11. Hydrostatic stress (σ_{cte}, σ_{trans} and σ_{tot}) as a function of the monoclinic phase content.

causes a tension stress on the alumina matrix that partially reduces the compressive stress originated by CTE mismatch. Furthermore, σ_{cte}, σ_{trans} and the overall hydrostatic (compressive) stress change linearly with monoclinic fraction as shown in Fig. 11, confirming experimental results previously reported by Sergo et al.[40]

4. Conclusions

Alumina–zirconia composites were extensively characterized in order to establish a correlation between mechanical properties (hardness and fracture toughness) and sintering process, stabilizer content, chromia addition, zirconia–alumina weight ratio and platelets reinforcement addition. Main results are:

1. The highest value of fracture toughness was achieved with pressureless sintering of the composite containing chromia 0.5 wt.% and yttria 2 mol%.
2. Post-hot isostatic pressing treatment caused the formation of a small quantity of monoclinic phase that reduced fracture toughness.
3. Transformability was strongly affected by stabilizer content.
4. Chromia addition led to an enhancement of the fracture toughness
5. A new magnetoplumbite type phase, $CeMgAl_{11}O_{19}$, was added to the composites. Preliminary results obtained with 20 wt.% addition confirmed that ZrO_2 toughening becomes less effective with these aluminates.
6. Stress-induced transformation toughening is the mechanism responsible for the fracture toughness improvement.
7. Overall compressive stress of the alumina grains is linearly dependent on monoclinic fraction and it can partially be reduced by the tensile stress originated by the t–m transformation.

Acknowledgements

This work was supported by the EU project GRD1-1999–10585 “HYPERCER”. The Authors wish to thank Dr. W. Burger (CeramTec-Plochingen, Germany) for the hot isostatic pressing and Dr. A. Stewart, Dr. C. Mingazzini, Mr. G.L. Minoccari and Mr. L. Beaulardi (ENEA-Faenza, Italy) for their helpful collaboration.

References

1. Claussen, N., Fracture toughness of Al_2O_3 with an unstabilized ZrO_2 dispersed phase. *J. Am. Ceram. Soc.*, 1976, **59**, 49–51.
2. Wang, J. and Stevens, R., Review—zirconia-toughened alumina (ZTA) ceramics. *J. Mater. Sci.*, 1989, **24**(10), 3421–3440.
3. Tsukuma, K., Ueda, K. and Shimada, M., Strength and fracture toughness of isostatically hot-pressed composites of Al_2O_3 and Y_2O_3 partially-stabilized ZrO_2. *J. Am. Ceram. Soc.*, 1985, **68**(1), C4–C5.
4. Tsukuma, K., Takahata, T. and Shiomi, M., Strength and fracture toughness of Y-TZP, Ce-TZP, Y-TZP/Al_2O_3, and Ce-TZP/Al_2O_3. *Advanced in Ceramics, Vol 24: Science and Technology of Zirconia III*. The American Ceramic Society, Columbus, OH, 1988, pp. 721–728.
5. Tuan, W. H., Chen, R. Z., Wang, T. C., Cheng, C. H. and Kuo, P. S., Mechanical properties of Al_2O_3/ZrO_2 composites. *J. Eur. Ceram. Soc.*, 2002, **22**(16), 2827–2833.
6. Shin, Y., Rhee, Y. and Kang, S., Experimental evaluation of toughening mechanism in alumina–zirconia composites. *J. Am. Ceram. Soc.*, 1999, **82**(5), 1229–1232.
7. Hannink, R. H. J., Kelly, P. M. and Muddle, B. C., Transformation toughening in zirconia-containing ceramics. *J. Am. Ceram. Soc.*, 2000, **83**(3), 461–487.
8. Garvie, R. C., The occurrence of metastable tetragonal zirconia as crystallite size effect. *J. Phys. Chem.*, 1965, **69**(4), 1238–1243.
9. Bhattacharyya, S. and Agrawal, D. C., Microstructure and mechanical properties of ZrO_2-Gd_2O_3 tetragonal polycrystals. *J. Mater. Sci.*, 2002, **37**(7), 1387–1394.
10. Tien, T. Y., *Toughened ceramics*. US Patent 4,886,768, 1989.
11. Jang, J. W., Kim, D. J. and Lee, D. Y., Size effect of trivalent oxides on low temperature phase stability of 2Y-TZP. *J. Mater. Sci.*, 2001, **36**(22), 5391–5395.
12. Lee, D. Y., Kim, D. and Cho, D., Low-temperature phase stability and mechanical properties of Y_2O_3- and Nb_2O_5-co-doped tetragonal zirconia polycrystal ceramics. *J. Mater. Sci. Lett.*, 1998, **17**(3), 185–187.
13. Khor, K. A. and Yang, Lattice parameters, tetragonality (*c*/*a*) and transformability of tetragonal zirconia phase in plasma sprayed ZrO_2-Er_2O_3 coatings. *Mater. Lett.*, 1997, **31**, 23–27.

14. Liu, X. Q. and Chen, X. M., Effects of $Sr_2Nb_2O_7$ additive on microstructure and mechanical properties of 3Y-TZP/Al_2O_3 ceramics. *Ceram. Int.*, 2002, **28**, 209–215.
15. Cutler, R. A., Mayhew, R. J., Prettyman, K. M. and Virkar, A. V., High-toughness Ce-TZP/Al_2O_3 ceramics with improved hardness and strength. *J. Am. Ceram. Soc.*, 1991, **74**(1), 179–186.
16. Yasuoka, M., Hirao, K., Brito, M. E. and Kanzaki, S., High-strength and high-fracture toughness ceramics in the Al_2O_3/$LaAl_{11}O_{18}$ system. *J. Am. Ceram. Soc.*, 1995, **78**(7), 1853–1856.
17. Chen, P. and Chen, I., In-situ alumina/aluminate platelet composites. *J. Am. Ceram. Soc.*, 1992, **75**(9), 2610–2612.
18. Guo, R., Guo, D., Chen, Y., Yang, Z. and Yuan, Q., In situ formation of $LaAl_{11}O_{18}$ rodlike particles in ZTA ceramics and effect on the mechanical properties. *Ceram. Int.*, 2002, **28**(7), 699–704.
19. Arahori, T., Suzuki, T., Iwamoto, N. and Umesaki, N., Transformation behaviour of ZrO_2 in Al_2O_3–ZrO_2 composites. *In Advanced in Ceramics, Vol 24: Science and Technology of Zirconia III*. The American Ceramic Society, Columbus, OH, 1988, pp. 549–554.
20. Kosmac, T., Wagner, R. and Claussen, N., X-ray determination of transformation depths in ceramics containing tetragonal ZrO_2. *J. Am. Ceram. Soc.*, 1981, **64**(4), C72–C73.
21. Gregori, G., Burger, W. and Sergo, V., Piezo-spectroscopic analysis of the residual stresses in zirconia-toughened alumina ceramics: the influence of the tetragonal-monoclinic transformation. *Mater. Sci. Eng. A*, 1999, **271**, 401–406.
22. Merlani, E., Schmid, C. and Sergo, V., Residual stresses in alumina/zirconia composites: effect of cooling rate and grain size. *J. Am. Ceram. Soc.*, 2001, **84**(12), 2962–2968.
23. Niihara, K., A fracture mechanism analysis of indentation-induced Palmqvist crack in ceramics. *J. Mater. Sci. Lett.*, 1983, **2**(5), 221–223.
24. Magnani, G., Sangiorgi, S., Stewart, A., Brillante, A. and Farina, L., Ottimizzazione della tenacità di materiali ceramici a base zirconia (TZP) con l'ausilio della spettroscopia Raman (in Italian). In *Proceedings IGF16, National Congress of Fracture Italian Group*, 2002.
25. Yoshimura, M., Yashima, M., Noma, T. and Somiya, S., Formation of diffusionlessly transformed tetragonal phases by rapid quenching of melts in ZrO_2–$RO_{1.5}$ systems (R = rare earths). *J. Mater. Sci.*, 1990, **25**(4), 2011–2016.
26. Ray, J. C., Saha, C. R. and Pramanik, P., Stabilized nanoparticles of metastable ZrO_2 with Cr^{3+}/Cr^{4+} cations: preparation from a polymer precursor and the study of the thermal and structural properties. *J. Eur. Ceram. Soc.*, 2002, **22**(6), 851–862.
27. Stefanic, G., Popovic, S. and Music, S., Influence of Cr_2O_3 on the stability of low temperature *t*-ZrO_2. *Mater. Lett.*, 1998, **36**(5/6), 240–244.
28. Arahori, T. and Whitney, D. E., Microstructure and mechanical properties of Al_2O_3–Cr_2O_3–ZrO_2 composites. *J. Mater. Sci.*, 1988, **23**(5), 1605–1609.
29. Babiarz, J. and Haberko, K., Cr_2O_3-doped Y-TZP composites. In *Proceedings ECERS '99, 6th European Ceramic Society Conference and Exhibition, British Ceramic Proceedings*, 1999, pp. 109–110.
30. Riu, D., Kong, Y. and Kim, H., Effect of Cr_2O_3 addition on microstructural evolution and mechanical properties of Al_2O_3. *J. Eur. Ceram. Soc.*, 2000, **20**(10), 1475–1481.
31. Hirata, T., Akiyama, K. and Yamamoto, H., Sintering behavior of Cr_2O_3–Al_2O_3 ceramics. *J. Eur. Ceram. Soc.*, 2000, **20**(2), 195–199.
32. McMeeking, R. M. and Evans, A. G., Mechanics of transformation-toughening in brittle materials. *J. Am. Ceram. Soc.*, 1982, **65**(5), 242–246.
33. Katagiri, G., Ishida, H., Ishitani, A. and Masaki, T., Direct determination by Raman microprobe of the transformation zone size in Y_2O_3 containing tetragonal ZrO_2 polycrystals. *In Advanced in Ceramics, Vol 24: Science and Technology of Zirconia III*. The American Ceramic Society, Columbus, OH, 1988, pp. 537–544.
34. Mori, Y., Kitano, Y., Ishitani, A. and Masaki, T., X-ray determination of transformation zone size in toughened zirconia ceramics. *J. Am. Ceram. Soc.*, 1988, **71**(7), C322–C324.
35. Swain, M. V. and Rose, L. R. F., Strength limitations of transformation-toughened zirconia alloys. *J. Am. Ceram. Soc.*, 1986, **69**(7), 511–518.
36. Gokhale, N. M., Dayal, R., Sharma, S. C. and Lal, R., Investigation on crystalline phases and mechanical properties of TZP ceramics prepared from sol-gel powders. *J. Mater. Sci.*, 1994, **29**(21), 5709–5714.
37. Grabner, L., Spectroscopic technique for the measurement of residual stress in sintered Al_2O_3. *J. Appl. Phys.*, 1978, **49**(2), 580–583.
38. Ma, Q. and Clarke, D. R., Stress measurement in single-crystal and polycrystalline ceramics using their optical fluorescence. *J. Am. Ceram. Soc.*, 1993, **76**(6), 1433–1440.
39. He, J. and Clarke, D. R., Determination of the piezospectroscopic coefficients for chromium-doped sapphire. *J. Am. Ceram. Soc.*, 1995, **78**(5), 1347–1353.
40. Sergo, V., Clarke, D. R. and Pompe, W., Deformation bands in ceria-stabilized tetragonal zirconia/alumina: I. Measurement of internal stresses. *J. Am. Ceram. Soc.*, 1995, **78**(3), 633–640.